Published in final edited form as:
J Pediatr Surg. 2013 June ; 48(6): 1330–1339. doi:10.1016/j.jpedsurg.2013.03.031.

Up-regulation of hypoxia-inducible factor 1 alpha and hemodynamic responses following massive small bowel resection☆,,☆☆

Kathryn J. Rowland[a,1], **Junjie Yao**[b,1], **Lidai Wang**[b], **Christopher R. Erwin**[a], **Konstantin I. Maslov**[b], **Lihong V. Wang**[b,*], and **Brad W. Warner**[a,*]

[a]Division of Pediatric Surgery, St Louis Children's Hospital, Department of Surgery, Washington University School of Medicine, St Louis, MO 63110, USA

[b]Optical Imaging Laboratory, Department of Biomedical Engineering, Washington University in St. Louis, St. Louis, MO 63130, USA

Abstract

Purpose—Massive small bowel resection (SBR) results in an adaptive response within the remnant bowel. We have previously shown an immediate reduction in intestinal blood flow and oxygen saturation (sO_2) after SBR. We therefore sought to determine the duration of resection-induced intestinal hypoxia and expression of hypoxia-inducible factors (HIFs) following SBR.

Methods—C57B6 mice were subjected to 50% proximal SBR or a sham procedure. Photoacoustic microscopy (PAM) was used to measure blood flow and sO_2 on postoperative days (PODs) 1, 3, and 7. Ileal tissue was harvested 6 h postoperatively and on PODs 1 and 2, and HIF1α, HIF2α, and VEGF mRNA expression were assessed via RT-PCR. A p value of less than 0.05 was considered significant.

Results—Following SBR, reduction in intestinal blood flow persists for 24 h and is followed with hyperemia by POD 3. The immediate reduction in venous sO_2 and increased tissue oxygen utilization continued through POD 7. Enhanced expression of HIF1α was demonstrated 6 h following SBR.

Conclusion—Massive SBR results in an immediate relative hypoxic state within the remnant bowel with early enhanced expression of HIF1α. On POD 7, increased tissue oxygen extraction and elevated blood flow persist in the adapting intestine.

Keywords

Small bowel resection (SBR); Intestine; Hypoxia-inducible factor; HIF1α; Oxygen saturation; Blood flow; Photoacoustic microscopy

☆Wang laboratory research was supported by the National Institutes of Health Grants R01 EB000712, R01 EB008085, R01 CA134539, U54 CA136398, R01 CA157277, and R01 CA159959. L.V. Wang has a financial interest in Microphotoacoustics, Inc. and Endra, Inc., which, however, did not support this work. K.I. Maslov has a financial interest in Microphotoacoustics, Inc., which, however, did not support this work.

☆☆Warner laboratory research was supported by National Institutes of Health Grants R01 DK059288 (Warner), T32 CA009621 (Rowland), and P30DK52574; Morphology and Murine Models Cores of the Digestive Diseases Research Core Center of the Washington University School of Medicine; and the St. Louis Children's Hospital Foundation–Children's Surgical Sciences Institute.

*Corresponding author. Tel.: +1 314 454 6022; fax: +1 314 454 2442. lhwang@biomed.wustl.edu (L.V. Wang), warnerb@wudosis.wustl.edu (B.W. Warner).
[1]These authors contributed equally to this work.

Short gut syndrome is a condition of high morbidity and mortality resulting from massive intestinal loss. In both human and animal models, massive small bowel resection (SBR) is followed by intestinal adaptation [1–3]. Adaptation compensates for the loss of bowel length via expansion of the nutrient absorptive surface area of the remnant bowel and is characterized by lengthening of the intestinal villi and deepening of the intestinal crypts.

Using photoacoustic microscopy (PAM), a non-invasive, label-free, high-resolution in vivo imaging modality, we recently demonstrated an immediate reduction in blood flow and oxygen saturation (sO_2) following SBR [4]. This relative hypoxic state was observed throughout the remnant small intestine and was accompanied by an increase in intestinal tissue oxygen extraction. The duration of these hemodynamic changes is presently unknown. Previous ex vivo studies of intestinal blood flow after SBR have demonstrated a variable hyperemic response as soon as 24 h post-resection; however, no studies have utilized an in vivo, real-time imaging system [5–7]. Using the animal's own endogenous hemoglobin as contrast, PAM is capable of anatomic, functional, and flow dynamic imaging and has been used to measure various hemodynamic parameters such as vessel density, vessel length, vessel tortuosity, total hemoglobin concentration, sO_2, blood flow speed, and the metabolic rate of oxygen [8–18].

The presence of villus angiogenesis in the adapted intestine on POD 7 following SBR has been previously established [19]. Hypoxia is a well-recognized trigger of angiogenesis and results in the activation of hypoxia-inducible factors (HIFs) responsible for the transcriptional activation or repression of hypoxic responsive genes [20,21]. HIF1a and HIF2α have nonredundant roles, and are functional as heterodimers, comprising a highly regulated, inducible alpha subunit and constitutive HIF1 beta subunit [22]. HIF1α and HIF2α are barely detectable in normoxic conditions, but become markedly up-regulated in hypoxic conditions [23]. Reoxygenation results in rapid degradation of HIF1a and HIF2α by the von Hippel–Lindau-mediated ubiquitin–proteosome system [24,25].

Intestinal epithelial cells have been shown to express both HIF1α and HIF2α [26]. HIF1α has been shown to be upregulated in states of intestinal mucosal inflammation, playing aprotective role [27–31]. Also, intestinal ischemia reperfusion models have demonstrated increased expression of HIF1a following ischemic insult [32]. HIF1α has also been demonstrated to be up-regulated in the presence of growth factors such as epidermal growth factor and insulin-like growth factor-1, cytokines such as interferon gamma, interleukin-1, and tumor necrosis factor-α, and exposure to *Pseudomonas aeruginosa* or bacterial lipopolysaccharide [32–38]. Activation of HIF1α results in many downstream effects, including activation of target genes responsible for angiogenesis, such as vascular endothelial growth factor (VEGF) [39–42]. HIF2α is responsive to decreases in intracellular iron as well as oxygen and has been implicated in regulation of the intestinal absorption of iron [26,43]. The response of HIF1α or HIF2α to the relative hypoxic state immediately following SBR is currently unknown. We therefore sought to determine the duration of resection-induced intestinal hypoxia and expression of hypoxia-inducible factors following SBR.

1. Materials and methods

1.1. Experimental design

Protocols for this study were approved by the Washington University Animal Studies Committee (20100103 for Warner and 20090275 for Wang) in accordance with the National Institutes of Health laboratory animal care and use guidelines. Mice underwent either 50% proximal SBR or a sham (enterotomy alone) procedure as previously described [1]. Photoacoustic microscopy measurements of vessel diameter, blood flow, and oxygen

saturation of the terminal mesenteric arteriole and accompanying vein were obtained at 6 cm proximal to the ileal–cecal junction (ICJ) on the serosal surface of the intestine. Measurements were compared to baseline reported previously and data acquired immediately (within minutes) after SBR and sham interventions [4].

1.2. Experimental animals

Male mice (C57BL/6; Harlan Laboratories, Inc., Indianapolis, IN) aged 7 to 16 weeks were used in this study. Mice were kept on a 12-h light–dark cycle and housed in a standard facility. One day prior to the procedure, the mice were placed on rodent liquid diet (Micro-Stabilized Rodent Liquid Diet LD101; Purina Mills, St Louis, MO).

1.3. Operative technique

Mice underwent 50% proximal SBR or sham operation (transection and reanastomosis only) as previously described [1]. Briefly, mice that underwent SBR had transection of the bowel at a point 12 cm proximal to the ICJ and also at a point 1 to 2 cm distal to the ligament of Treitz. The mesentery was ligated and the intervening bowel was removed. Intestinal continuity was restored with an end-to-end anastomosis using 9-0 monofilament suture. In mice undergoing sham operation the bowel was transected at a point 12 cm proximal to the ICJ and intestinal continuity was restored with an end-to-end reanastomosis. Following the operation, mice were provided free access to water for the first 24 h and were then given a liquid rodent diet until sacrifice.

1.4. Intestinal sO_2 and blood flow measured byphotoacoustic microscopy

Optical-resolution photoacoustic microscopy (OR-PAM) was used throughout this study as previously described and shown in Fig. 1A [4,11]. Briefly, short laser pulses are focused into the tissue by a set of optical components. The resulting photoacoustic signals are detected by an ultrasonic transducer (V214-BC, Olympus NDT) placed confocally with the optical objective. The animal is translated by a 2D scanning stage (PS-85, PI-Micros). An acoustic-optical beam combiner is composed of two prisms sandwiching a layer of silicone oil. The OR-PAM has been demonstrated to be capable of functional and flow dynamic imaging with capillary resolution (transverse: 2.5 μm, axial: 15 μm). An imaging depth of ~1.2 mm has been achieved in biological tissue. Because the two forms of hemoglobin (oxy-hemoglobin HbO_2 and deoxy-hemoglobin HbR) have distinct absorption spectra (Fig. 1B), the relative concentrations of HbO_2 and HbR can be quantified through spectral analysis of the PAM measurements at two or more wavelengths, and thus sO_2 can be computed [15].

During the experiment, mice were anesthetized with isoflurane (E-Z Anesthesia, Euthanex) on PODs 1, 3, and 7 and placed in a supine position on a heating pad (37 °C). A midline laparotomy was performed, and the entirety of the small bowel was exposed. The terminal mesenteric arteriole and accompanying vein at a point approximately 6 cm proximal to the ICJ was identified. Baseline sO_2 was measured on a $0.5 \times 1\text{-mm}^2$ area containing such vessel pairs at two optical wavelengths of 570 and 578 nm. Baseline blood flow speed was then measured at both locations across the proximal end of the vessel in M-mode using a bandwidth broadening based method [13,14]. The laser repetition rate was 6 kHz, and 2000 A-lines were acquired at each position. The area of the bowel not being measured was kept moistened with a normal saline soaked gauze pad. Following all measurements, the bowel was flushed with ice-cold PBS, excised, and the first 1-cm segment of bowel distal to the anastomosis was discarded. The next 2-cm segment of bowel was fixed in 10% neutral-buffered formalin for histology and the remaining distal bowel was discarded. The animal was then sacrificed via cervical dislocation.

1.5. Adaptation measurements

Villus height and crypt depth were measured on H&E-stained sections by a single investigator blinded to mouse strain or procedure using the image analysis software MetaMorph (Dowington, PA). Histology was obtained only for POD 3 and POD 7 animals, as we have previously demonstrated no consistent changes in histological morphology on POD 1 [1]. At least 20 well-oriented villi and crypt per animal were measured. Adaptation in the SBR animals was defined as a 20% increase in villus height as compared to the mean villus height of the POD 3 and 7 sham animals, and SBR animals that failed to meet adaptive criteria were excluded from further analysis [2].

1.6. Ileal tissue harvest for RT-PCR

At 6 h from initiation of the SBR or sham procedure and on PODs 1 and 2, the mice were anesthetized with isoflurane. A midline laparotomy was performed and the small bowel was flushed with ice-cold phosphate-buffered saline with protease inhibitors (0.2 mM phenylmethylsulfonyl fluoride, 5 μg/mL aprotinin, 1 mM benzamidine, 1 mM sodium orthovanadate, and 2 μM cantharidin; EMD, Gibbstown, NJ) and excised. The first 1-cm segment of bowel distal to the anastomosis was discarded. The next 2-cm segment of bowel from the POD 7 mice was fixed in 10% neutral-buffered formalin for histology. Bowel from the six hour timepoint and POD 1 was not collected for histology as we have previously shown no evidence of histological adaptation prior to POD 3. The subsequent 5 cm of bowel was cut longitudinally and transferred into tubes containing 5 mL of ice-cold PBS with protease inhibitors for 1 h at 4 °C. Crypt and villus enterocytes and the underlying mesenchymal/muscularis layer were isolated using a calcium chelation, mechanical vibration, and cell straining protocol that we have beforehand described [44].

1.7. RT-PCR of HIF1α, VEGF, and HIF2α

Total RNA was extracted from frozen isolated crypt and villus enterocytes and underlying mesenchymal/muscularis fractions following the manufacturer's protocol for the RNAqueous kit (Ambion, Austin, TX), and total RNA concentration was determined spectrophotometrically. The quality of the obtained RNA was evaluated using the Bio-Rad Experion System with an RNA StdSens Chip and reagents (Bio-Rad Laboratories, Richmond, CA). RNA samples that showed no significant degradation were used directly in a TaqMan RNA-to Cr 1-Step Kit (Applied Biosystems, Foster City, CA). Primers for HIF1α, HIF2α, VEGF and β-actin, which was used as the endogenous control, were obtained from Applied Biosystems (Foster City, CA). All samples were run in triplicate and a standard whole bowel sample was used as the calibrator. An Applied Biosystems 750 Fast Real-Time PCR System (Foster City, CA) was used to run the samples.

1.8. Statistical analysis

All photoacoustic data processes were conducted using MATLAB (R2008a, MathWorks). Quantitative values are presented as mean ± SEM. An unpaired Student's *t*-test was used for comparisons between all measurements. A p value less than 0.05 was considered statistically significant. The Sigma Stat statistical package (SPSS, Chicago, IL) was used for all statistical analyses.

2. Results

2.1. Photoacoustic microscopy

A total of 7 POD 1, 9 POD 3, and 8 POD 7 mice underwent the SBR procedure with post-SBR measurements, and 7 POD 1, 8 POD 3, and 9 POD 7 mice underwent the sham procedure with post-sham measurements. One POD 1 SBR mouse was excluded from

further analysis as both the sO_2 and blood flow measurements for the animal were far greater than two standard deviations from the mean of the remaining animals.

2.2. Adaptation measurements

As expected, SBR resulted in an increase in villus height as compared to sham on POD 7 (297 ± 7.4 vs. 217 ± 6.8, $p = 0.000002$) and POD 3 (303 ± 11.7 vs. 227 ±10.1, $p = 0.0004$). Crypt depth was increased on POD 7 following SBR as compared to sham (115 ±4.1 vs. 92.7 ± 5.3, $p = 0.007$), with a trend toward increased SBR crypt depth on POD 3 (128 ± 12.2 vs. 103 ± 5.9, $p = 0.067$). Three POD 3 SBR animals and one POD 7 SBR animal were excluded from further PAM measurement analysis as they failed to demonstrate histological evidence for normal adaptation.

2.3. Arterial and venous oxygen saturation

Typical sO_2 images following SBR and sham are shown in Fig. 1C. Arterial sO_2 decreased immediately following SBR as compared to preoperative levels and remained decreased through POD 1, with a statistically significant decrease in arterial sO_2 between SBR and sham on POD 1 (Fig. 2A). Venous sO_2 also decreased immediately following SBR as compared to preoperative levels and remained decreased through POD 7 (Fig. 2B), with a significantly lower venous sO_2 post-SBR as compared to sham data observed immediately and on PODs 3 and 7.

2.4. Tissue oxygen extraction

Tissue oxygen extraction fraction (OEF) is defined as $(\mathrm{sO}_2^{\mathrm{artery}} - \mathrm{sO}_2^{\mathrm{vein}})/\mathrm{sO}_2^{\mathrm{artery}}$ and represents the fraction of O_2 molecules that cross the capillary wall in a steady state. OEF was immediately increased post-SBR as compared to preoperative levels and remained elevated through POD 7 (Fig. 3). The sham procedure also resulted in a significant increase in OEF as compared to preoperative levels, however to a lesser magnitude than that observed following SBR.

2.5. Arterial and venous blood flow

Arterial blood flow decreased immediately following SBR as compared to preoperative levels, which, however recovered by POD 1 (Fig. 4A). As compared to sham, arterial blood flow was significantly lower immediately post-SBR and significantly higher on PODs 3 and 7. Venous blood flow also decreased immediately following SBR as compared to preoperative levels, and recovered by POD 1 (Fig. 4B). As compared to sham, venous blood flow was significantly lower immediately post-SBR and significantly higher on SBR POD 7.

2.6. RT-PCR

Ileal tissue harvested from a total of six animals 6 h following SBR, six POD 1 SBR, and four POD 2 SBR was analyzed and compared to tissue from six animals 6 h following sham, seen POD 1 sham, and three POD 2 sham. Ileal tissue from six unoperated animals was also used for comparison.

2.7. HIF1α expression

Initial RT-PCR for HIF1α on POD 3 and 7 failed to show any prominent differences from unoperated intestine, leading us to look at earlier time points (data not shown). HIF1α was significantly up-regulated in the mesenchymal/muscularis layer of the intestine following both the SBR and sham procedure at 6 h postop and on POD 1 (Fig. 5A). By POD 2, HIF1α expression in the mesenchymal/muscularis layer returned to unoperated levels in both the SBR and sham animals. No statistically significant difference was seen in HIF1α expression

between the SBR and sham animals in the mesenchymal/muscularis layer at any experimental time point. HIF1α expression in the crypt and villus fractions was also investigated. While SBR and sham animals demonstrated differences in expression from unoperated tissue, these enterocyte cellular fractions failed to demonstrate the magnitude of response as seen in the mesenchymal/muscularis layer (data not shown).

2.8. HIF2α expression

HIF2a was significantly up-regulated 6 h post-sham in the mesenchymal/muscularis layer with a trend toward up-regulation in the post-SBR animals, as compared to unoperated tissue (Fig. 5B). This was followed by a significant down-regulation of HIF2α following SBR and sham on POD 1, as compared to unoperated tissue. In the SBR animals, this down-regulation persisted on POD 2. No statistically significant difference was seen in HIF2α expression between the SBR and sham animals in the mesenchymal/muscularis layer at any experimental time point.

2.9. VEGF expression

VEGF expression was significantly down-regulated in the mesenchymal/muscularis layer at 6 h post-SBR and sham as compared to unoperated tissue (Fig. 5C). No differences in expression were observed on POD 1 or 2 in the SBR or sham animals as compared to unoperated tissue. No statistically significant difference was seen in VEGF expression between the SBR and sham animals in the mesenchymal/muscularis layer at any experimental time point.

3. Discussion

SBR results in villus angiogenesis and intestinal adaptation [1,19]. The immediate, relative hypoxic environment following SBR has been previously reported and is manifested by decreased blood flow, decreased oxygen saturation, and increased tissue oxygen extraction [4]. The results of our present study demonstrate that this hypoxic environment is accompanied by early up-regulation of HIF1α and followed by a later increase in intestinal blood flow consistent with angiogenesis.

The hemodynamic changes observed following SBR demonstrate a persistent elevated tissue oxygen extraction in the remnant bowel through POD 7. This increased tissue oxygen requirement within the adapting intestine is not surprising given the known increase in proliferation of cells that occurs in adaptation [1,2]. The sham animals also demonstrated an increase in tissue oxygen extraction following enterotomy alone; however, this increase was not to the magnitude of that following resection. The increased tissue oxygen extraction following sham may therefore reflect the metabolic activity associated with repair and healing of the bowel anastomosis and/or stress of an operative procedure involving all cells of the body.

We have presently demonstrated an elevation in blood flow beginning on POD 3 following SBR. It is during this same time that the histological changes associated with adaptation (lengthening of the villi and deepening of the crypts) are first observed [1,2]. By POD 7 increased villus capillary networks are well established [19]. The observed elevation in blood flow may serve to support such new vessel growth. Our observations of post-SBR hyperemia are consistent with those previously reported using ex vivo methods of measurement, although the timing and duration of increased flow vary by report [5–7].

Our analysis of genetic changes that result from the immediate relative hypoxic environment following SBR demonstrates that HIF1α is up-regulated early, at 6 h post-SBR and remains elevated on POD 1. HIF1a is known to play a role in intestinal colitis and ischemia

reperfusion injury models. Mice with intestinal epithelial cell specific expression of mutant HIF1α, resulting in loss of function, have more severe clinical symptoms of colitis with loss of gut barrier function and amplified intestinal inflammation, while overexpression of epithelial HIF1α is protective for these measures [27]. Inhibition of the enzymes that degrade HIF has also shown a protective effect in murine colitis models [28–31]. Intestinal ischemia reperfusion models have supported both protective and deleterious roles for HIF1α [45–47]. The different roles for HIF1α in these models may be due to the duration and severity of ischemia [47].

We were surprised to note that the sham procedure was followed by an equivalent degree of HIF1α up-regulation as seen following SBR. This suggests that HIF1α alone is not responsible for the adaptation hemodynamic changes seen post-SBR. Alternatively, it must be considered that changes in HIF1α expression may have a differential effect on downstream targets in the SBR setting as compared to sham. Surprisingly, VEGF, a major downstream target for HIF1α was not up-regulated in response to SBR or sham. In fact, VEGF mRNA expression was decreased at 6 h post-procedure. Using PAM, VEGF has been established to be essential in epithelial cells for HIF1α mediated neovascularization, but is not required for the angiogenic process of endothelial sprouting [48]. Within the intestine, VEGF has been previously determined to be critical for a complete histological adaptive response to SBR and has been shown to increase the vascular density in the adapting bowel [49]. However, the timing and degree of VEGF expression following SBR in order for a complete adaptive response to occur are presently unknown.

In this study we have demonstrated a significant decrease in HIF2α expression in the ileum on POD 1 following SBR and sham. Both HIF1α and HIF2α are capable of activating transcription of VEGF, although the expression of and response to HIF is cell and organ specific [50]. HIF1α deficiency and HIF2α deficiency are embryonic lethal [51–55]. While HIF2α deficient fetal lung tissue demonstrated reduced VEGF levels [55], culture of HIF2α-deficient embryonic kidney cells showed persistent VEGF mRNA levels despite loss of HIF2α [56]. Our observed decreased VEGF mRNA levels preceded the decline in HIF2α, making it unlikely that the decreased expression of HIF2α accounts for the observed effect on expression of VEGF. The physiological significance of HIF2α down-regulation is unclear at this time. In intestinal cells, HIF2α has been implicated mainly in regulating duodenal iron absorption [26,43].

Further work in the SBR model is necessary to determine the role that HIF1α and HIF2α play post-SBR. While hypoxia and HIF1α expression are present in the early post-SBR environment, HIF1α alone is unable to account for the angiogenic adaptation response seen following SBR. By POD 7 following SBR, the adapted intestine is characterized by not only an increase in crypt depth and villus height, but by elevated intestinal blood flow and increased tissue oxygen extraction. It is possible that alterations in HIF1α and/or HIF2a expression promote such hemodynamic changes and may therefore serve as potential therapeutic targets in short gut syndrome, helping to encourage intestinal adaptation.

References

1. Helmrath MA, VanderKolk WE, Can G, et al. Intestinal adaptation following massive small bowel resection in the mouse. J Am Coll Surg. 1996; 183:441–9. [PubMed: 8912612]
2. Taylor JA, Martin CA, Nair R, et al. Lessons learned: optimization of a murine small bowel resection model. J Pediatr Surg. 2008; 43:1018–24. [PubMed: 18558176]
3. McDuffie LA, Bucher BT, Erwin CR, et al. Intestinal adaptation after small bowel resection in human infants. J Pediatr Surg. 2011; 46(6):1045–51. [PubMed: 21683196]

4. Rowland KJ, Yao J, Wang L, et al. Intestinal oxygen saturation and blood flow decrease immediately following massive small bowel resection. J Pediatr Surg. 2012; 47(6):1143–9. [PubMed: 22703784]
5. Ulrich-Baker MG, Hollwarth ME, Kvietys PR, et al. Blood flow responses to small bowel resection. Am J Physiol. 1986; 251(6):G815–22. [PubMed: 3789147]
6. Touloukian RJ, Spencer RP. Ileal blood flow preceding compensatory intestinal hypertrophy. Ann Surg. 1972; 175(3):320–5. [PubMed: 5077796]
7. Jesseph JE, Jacklin AJ. Effects of partial resection of mammalian small intestine. III. Glucose absorption, CO2 production and blood flow in residual ileum in the dog. Rev Surg. 1963; 20:384–7. [PubMed: 14077529]
8. Kim C, Favazza C, Wang LV. In vivo photacoustic tomography of chemicals: high-resolution functional and molecular optical imaging at new depths. Chem Rev. 2010; 110(5):2756–82. [PubMed: 20210338]
9. Yao J, Maslov K, Hu S, et al. Evans blue dye-enhanced capillary resolution photacoustic microscopy in vivo. J Biomed Opt. 2009; 14(5):054049. [PubMed: 19895150]
10. Maslov K, Zhang HF, Hu S, et al. Optical-resolution photoacoustic microscopy for in vivo imaging of single capillaries. Opt Lett. 2008; 33(9):929–31. [PubMed: 18451942]
11. Wang L, Maslov K, Yao J, et al. Fast voice-coil scanning optical-resolution photoacoustic microscopy. Opt Lett. 2011; 36(2):139–41. [PubMed: 21263479]
12. Wang X, Pang Y, Ku G, et al. Noninvasive laser-induced photoacoustic tomography for structural and functional in vivo imaging of the brain. Nat Biotechnol. 2003; 21(7):803–6. [PubMed: 12808463]
13. Yao J, Maslov KI, Shi Y, et al. In vivo photoacoustic imaging of transverse blood flow by using Doppler broadening of bandwidth. Opt Lett. 2010; 35(9):1419–21. [PubMed: 20436589]
14. Yao J, Wang LV. Transverse flow imaging based of photoacoustic Doppler badwidth broadening. J Biomed Opt. 2010; 15(2):021304. [PubMed: 20459226]
15. Zhang HF, Maslov K, Sivaramakrishnan M, et al. Imaging of hemoglobin oxygen saturation variations in single vessels in vivo using photoacoustic microscopy. Appl Phys Lett. 2007; 90(5): 053901.
16. Zhang HF, Maslov K, Stoica G, et al. Functional photoacoustic microscopy for high-resolution and noninvasive in vivo imaging. Nat Biotechnol. 2006; 24(7):848–51. [PubMed: 16823374]
17. Yao J, Maslov KI, Zhang Y, et al. Label-free oxygen-metabolic photoacoustic microscopy in vivo. J Biomed Opt. 2011; 16(7):076003–11. [PubMed: 21806264]
18. Zhang C, Maslov K, Wang LV. Subwavelength-resolution label-free photacoustic microscopy of optical absorption in vivo. Opt Lett. 2010; 35(19):3195–7. [PubMed: 20890331]
19. Martin CA, Perrone EE, Longshore SW, et al. Intestinal resection induces angiogenesis within adapting intestinal villi. J Pediatr Surg. 2009; 44(6):1077–82. [PubMed: 19524720]
20. Cassavaugh J, Lounsbury KM. Hypoxia-mediated biological control. J Cell Biochem. 2011; 112(3):735–44. [PubMed: 21328446]
21. Wang GL, Jiang BH, Rue EA, Semenza GL. Hypoxia-inducible factor 1 is a basic-helix-loop-helix-PAS heterodimer regulated by cellular O_2 tension. Proc Natl Acad Sci USA. 1995; 92(12): 5510–4. [PubMed: 7539918]
22. Radcliffe PJ. HIF-1 and HIF-2; working alone or together in hypoxia? J Clin Invest. 2007; 117:862–5. [PubMed: 17404612]
23. Huang LE, Arany Z, Livingston DM, et al. Activation of hypoxia-inducible transcription factor depends primarily upon redox-sensitive stabilization of its alpha subunit. J Biol Chem. 1996; 271:32253–9. [PubMed: 8943284]
24. Maxwell PH, Wiesener MS, Chang GW, et al. The tumour suppressor protein VHL targets hypoxia-inducible factors for oxygen-dependent proteolysis. Nature. 1999; 399(6733):271–5. [PubMed: 10353251]
25. Epstein AC, Gleadle JM, McNeill LA, et al. *C. elegans* EG:-9 and mammalian homologs define a family of dioxygenases that regulate HIF by prolyl hydroxylation. Cell. 2001; 107(1):43–54. [PubMed: 11595184]

26. Mastrogiannaki M, Matak P, Keith B, et al. HIF-2alpha, but not HIF-1alpha, promotes iron absorption in mice. J Clin Invest. 2009; 119(5):1159–66. [PubMed: 19352007]
27. Karhausen J, Furuta GT, Tomaszewski JE, et al. Epithelial hypoxia-inducible factor-1 is protective in murine experimental colitis. J Clin Invest. 2004; 114(8):1098–106. [PubMed: 15489957]
28. Kaelin WG Jr, Ratcliffe PJ. Oxygen sensing by metazoans; the central role of the HIF hydroxylase pathway. Mol Cell. 2008; 30:393–402. [PubMed: 18498744]
29. Cummins EP, Seeballuck F, Keely SJ, et al. The hydroxylase inhibitor dimethyloxalyglycine is protective in murine models of colitis. Gastroenterology. 2008; 143:156–65. [PubMed: 18166353]
30. Robinson A, Keely S, Karhausen J, et al. Mucosal protection by hypoxia-inducible factor prolyl hydroxylase inhibition. Gastroenterology. 2008; 134:145–55. [PubMed: 18166352]
31. Tambuwala MM, Cummins EP, Lenihan CR, et al. Loss of prolyl hydroxylase-1 protects against colitis through reduced epithelial cell apoptosis and increased barrier function. Gastroenterology. 2010; 139:2093–101. [PubMed: 20600011]
32. Kuory J, Deitch EA, Homma H, et al. Persistent HIF-1a activation in gut ischemia/reperfusion injury: potential role of bacteria and lipopolysaccharide. Shock. 2004; 22:270–7. [PubMed: 15316398]
33. Fukuda R, Hirota K, Fan F, et al. Insulin-like growth factor 1 induces hypoxia-inducible factor 1-mediated vascular endothelial growth factor expression, which is dependent on MAP kinase and phospati-dylinositol 3-kinase signaling in colon cancer cells. Biol Chem. 2002; 277(41):38205–11.
34. Fukada R, Kelly B, Semenza GL. Vascular endothelial growth factor gene expression in colon cancer cells exposed to prostaglandin E2 is mediated by hypoxia-inducible factor 1. Cancer Res. 2003; 63(9):2330–4. [PubMed: 12727858]
35. Feldser D, Agani F, Iyer NV, et al. Reciprocal positive regulation of hypoxia-inducible factor 1alpha and insulin-like growth factor 2. Cancer Res. 1999; 59(16):3915–8. [PubMed: 10463582]
36. Scharte M, Han X, Bertges DJ, et al. Cytokines induce HIF-1 DNA binding and the expression of HIF-1-dependent genes in cultured rat enterocytes. Am J Physiol Gastrointest Liver Physiol. 2003; 284:G373–84. [PubMed: 12388200]
37. Kuniyasu H, Chihara Y, Kondo H. A role of histone H4 hypoacetylation in vascular endothelial growth factor expression in colon mucosa adjacent to implanted cancer in athymic mice cecum. Pathobiology. 2002-2003; 70(6):348–352. [PubMed: 12865631]
38. Thornton RD, Lane P, Borghaei RC, et al. Interleukin 1 induces hypoxia-inducible factor 1 in human gingival and synovial fibroblasts. Biochem J. 2000; 350:307–12. [PubMed: 10926858]
39. Shweiki D, Itin A, Soffer D, et al. Vascular endothelial growth factor induced by hypoxia may mediate hypoxia-initiated angiogenesis. Nature. 1992; 359(6398):843–5. [PubMed: 1279431]
40. Semenza GL. Life with oxygen. Science. 2007; 318:62–4. [PubMed: 17916722]
41. Levy AP, Levy NS, Wegner S, et al. Transcriptional regulation of the rat vascular endothelial growth factor gene by hypoxia. J Biol Chem. 1995; 270:13333–40. [PubMed: 7768934]
42. Liu Y, Cox SR, Morita T, et al. Hypoxia regulates VEGF expression in endothelial cells: identification of a 5′ enhancer. Circ Res. 1995; 77:638–43. [PubMed: 7641334]
43. Shah YM, Matsubara T, Ito S, et al. Intestinal hypoxia-inducible transcription factors are essential for iron absorption following iron deficiency. Cell Metab. 2009; 9(2):152–64. [PubMed: 19147412]
44. Guo J, Longshore S, Nair R, et al. Retinoblastoma protein (pRb), but not p107 or p130, is required for maintenance of enterocyte quiescence and differentiation in small intestine. J Biol Chem. 2009; 284(1):134–40. [PubMed: 18981186]
45. Hart ML, Henn M, Kohler D, et al. Role of extracellular nucleotide phosphydrolysis in intestinal ischemia-reperfusion injury. FASEB J. 2008; 22:2784–97. [PubMed: 18353866]
46. Hart ML, Jacobi B, Schittenhelm J, et al. Cutting edge: A2B adenosine receptor signaling provides potent protection during intestinal ischemia/reperfusion injury. J Immunol. 2009; 182:3965–8. [PubMed: 19299692]
47. Kolenkode BK, Colorado I, Reino D, et al. Hypoxia-inducible factor plays a gut-injurious role in intestinal ischemia reperfusion injury. Am J Physiol Gastrointest Liver Physiol. 2010; 300:G853–861. [PubMed: 21183660]

48. Oladipupo S, Hu S, Kovalski J, et al. VEGF is essential for hypoxia-inducible factor-mediated neovascularization but dispensable for endothelial sprouting. Proc Natl Acad Sci USA. 2011; 108(32):13264–9. [PubMed: 21784979]

49. Parvadia JK, Keswani SG, Vaikunth S, et al. Role for VEGF in small bowel adaptation after resection: the adaptive response is angiogenesis dependent. Am J Physiol Gastrointest Liver Physiol. 2007; 293:G591–598. [PubMed: 17585015]

50. Freeburg PB, Rpbert B, St John PL, et al. Podocyte expression of hypoxia-inducible factor (HIF)-1 and HIF-2 during glomerular development. J Am Soc Nephrol. 2003; 14:927–38. [PubMed: 12660327]

51. Iyer NV, Kotch LE, Agani F, et al. Cellular and developmental control of O_2 homeostasis by hypoxia-inducible factor 1a. Genes Dev. 1998; 12:149–62. [PubMed: 9436976]

52. Ryan HE, Lo J, Johnson RS. HIF-1a is required for solid tumor formation and embryonic vascularization. EMBO J. 1998; 17:3003–15.

53. Peng J, Zhang L, Drysdale L, et al. The transcription factor EPAS-1/hypoxia-inducible factor 2alpha plays an important role in vascular remodeling. Proc Natl Acad Sci USA. 2000; 97:8386–91. [PubMed: 10880563]

54. Tian H, Hammer RE, Matsumoto AM, et al. The hypoxia-responsive transcription factor EPAS1 is essential for catecholamine homeostasis and protection against heart failure during embryonic development. Genes Dev. 1998; 12:3320–4. [PubMed: 9808618]

55. Compernolle V, Brusselmans K, Acker T, et al. Loss of HIF-2alpha and inhibition of VEGF impair fetal lung maturation, whereas treatment with VEGF prevents fatal respiratory distress in premature mice. Nat Med. 2002; 8:702–10. [PubMed: 12053176]

56. Steenhard BM, Freeburg PB, Isom K, et al. Kidney development and gene expression in HIF2a knockout mice. Dev Dyn. 2007; 236(4):1115–25. [PubMed: 17342756]

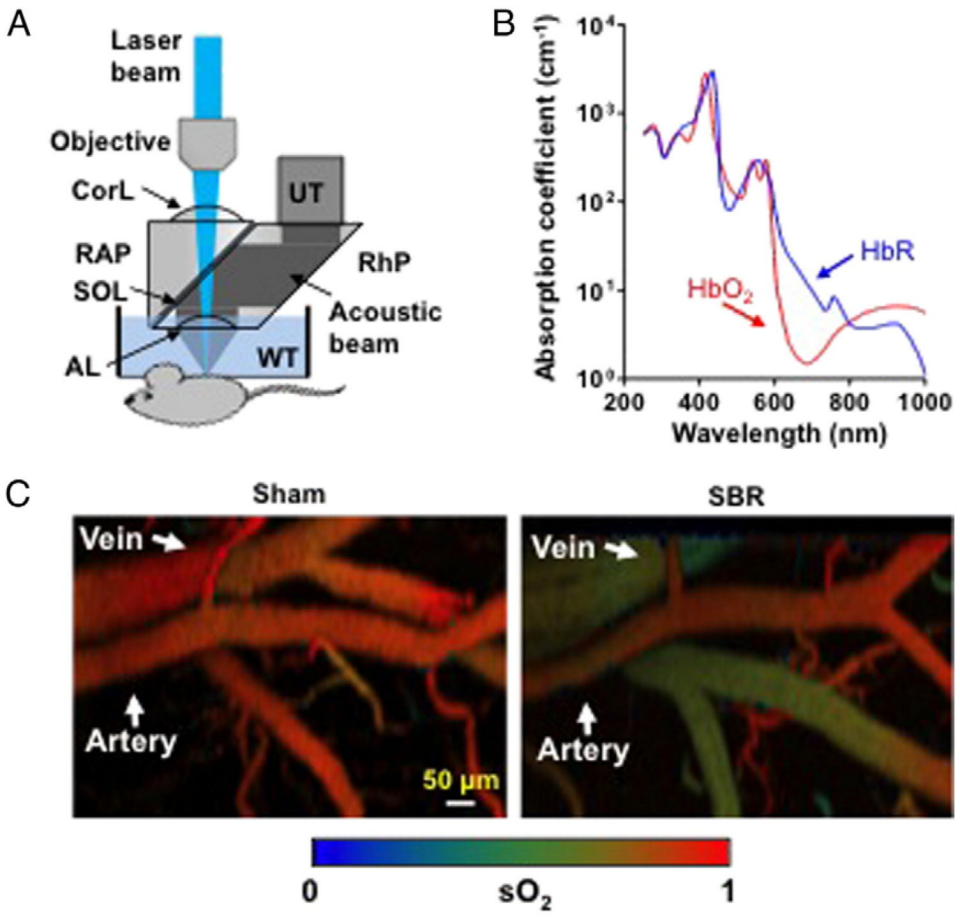

Fig. 1.

Photoacoustic microscopy of hemodynamic responses following small bowel resection (SBR) or sham (bowel transection and reanastomosis alone). (A) Schematic of the optical-resolution photoacoustic microscopy system, where a lateral resolution of 2.5 μm is achieved by the diffraction-limited optical focusing. AL, acoustic lens; Corl, correction lens; RAP, right angled prism; RhP, rhomboid prism; SOL, silicone oil layer; UT, ultrasonic transducer; WT, water tank. (B) Absorption spectra of oxy-hemoglobin (HbO_2) and deoxy-hemoglobin (HbR) (150 g/L in blood), allowing for oxygen saturation (sO_2) calculation. (C) Representative intestinal sO_2 images following SBR and sham.

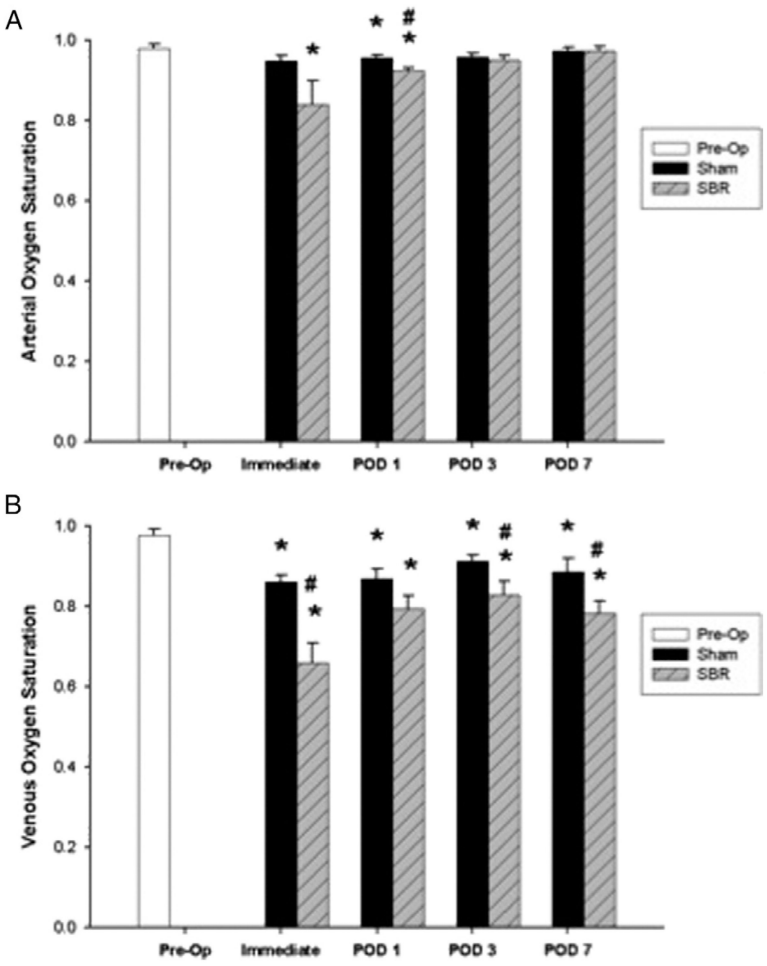

Fig. 2.

Oxygen saturation (sO_2) of the terminal mesenteric arteriole (A) and accompanying vein (B) preoperatively and immediately (within fifteen minutes), postoperative day (POD) 1, POD 3, and POD 7 following sham and 50% proximal small bowel resection (SBR) at a location 6 cm from the ileal–cecal junction. Asterisk indicates $p < 0.05$ as compared to preop (preop vs. sham and preop vs. SBR). Number sign indicates $p < 0.05$ for sham vs. SBR.

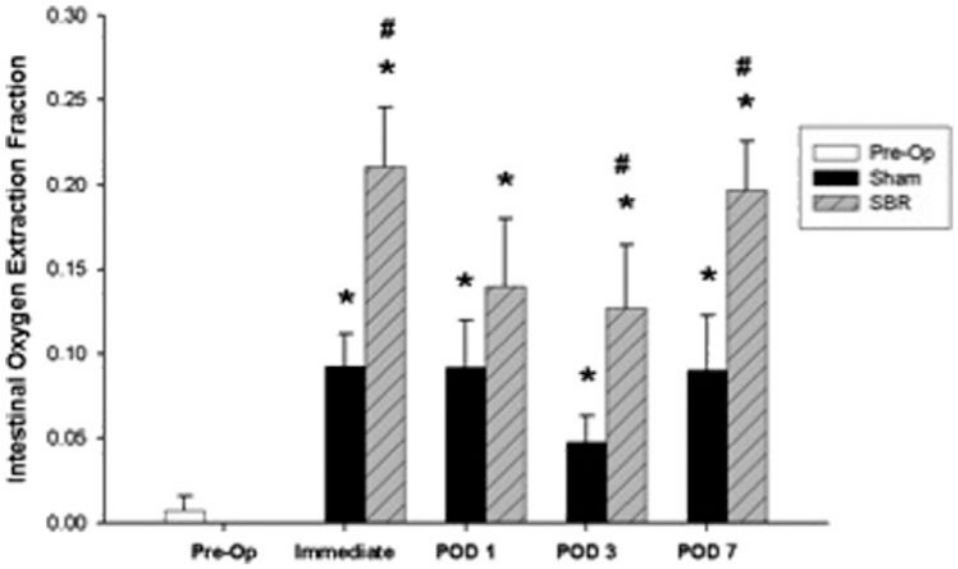

Fig. 3.

Tissue oxygen extraction fraction preoperatively and immediately (within 15 min), postoperative day (POD) 1, POD 3, and POD 7 following sham and 50% proximal small bowel resection (SBR) at a location 6 cm from the ileal–cecal junction. Asterisk indicates $p < 0.05$ as compared to preop (preop vs. sham and preop vs. SBR). Number sign indicates $p < 0.05$ for sham vs. SBR.

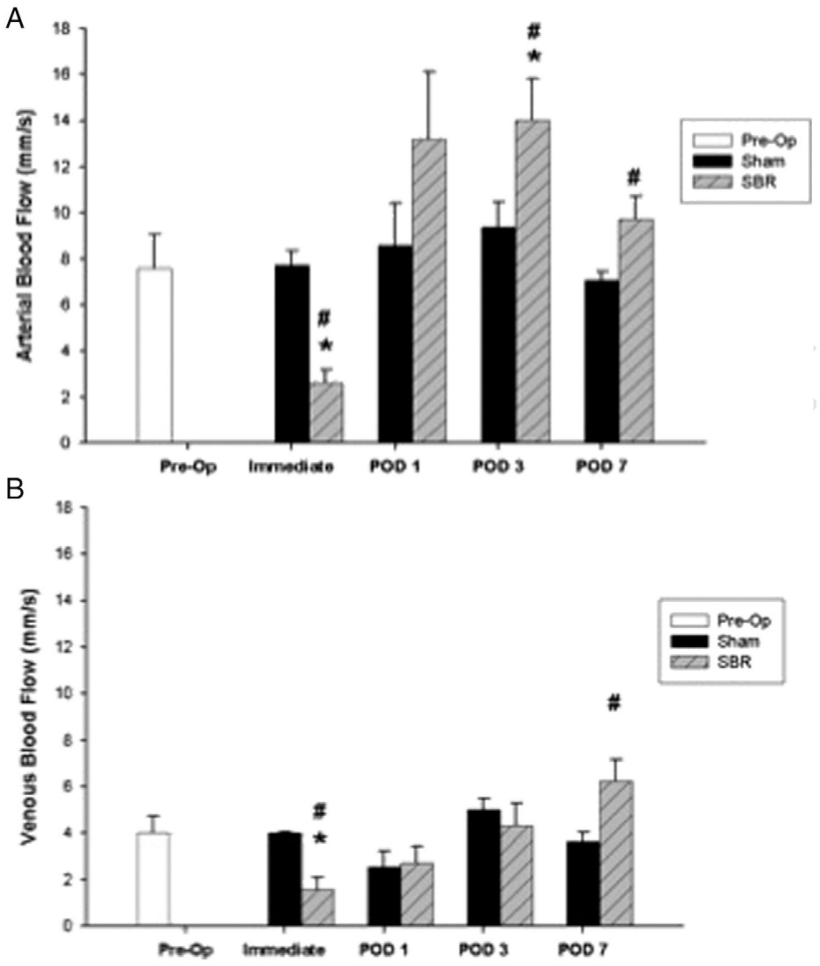

Fig. 4.

Blood flow (mm/s) of the terminal mesenteric arteriole (A) and accompanying vein (B) preoperatively and immediately (within 15 min), postoperative day (POD)1, POD 3, and POD 7 following sham and 50% proximal small bowel resection (SBR) at a location 6 cm from the ileal–cecal junction. Asterisk indicates $p < 0.05$ as compared to preop (preop vs. sham and preop vs. SBR). Number sign indicates $p < 0.05$ for sham vs. SBR.

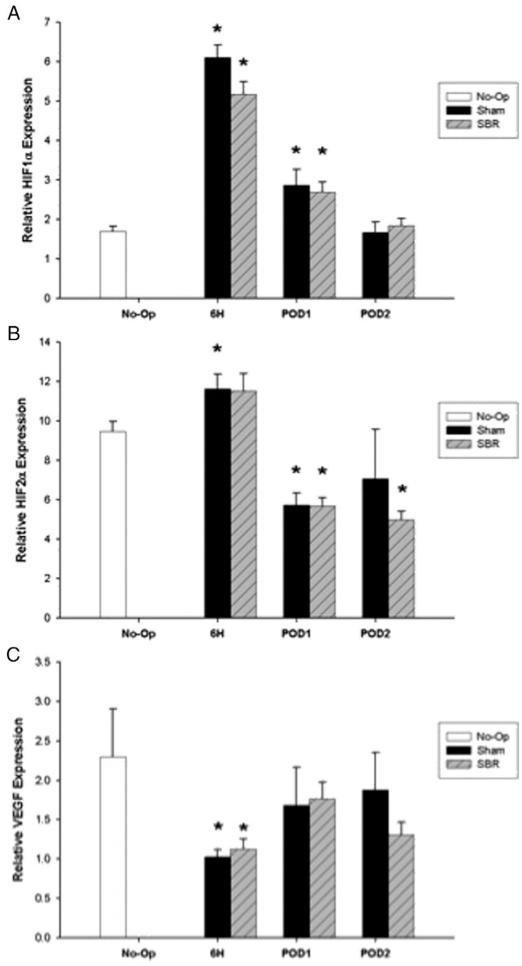

Fig. 5.

TaqMan real-time PCR for HIF1α (A), HIF2α (B), and VEGF (C) mRNA in the mesenchyme/muscularis layer of the intestine for unoperated and 6 h postoperative, postoperative day (POD) 1, and POD 2 following sham and 50% proximal small bowel resection (SBR). Asterisk indicates $p < 0.05$ as compared to unoperated (unoperated vs. sham and unoperated vs. SBR).